Available online at www.sciencedirect.com

ScienceDirect

Ceramics International 39 (2013) 9157–9161

CERAMICS INTERNATIONAL

www.elsevier.com/locate/ceramint

Contour mapping 2D and 3D-photoluminescence of Au-doped one-dimensional Eu(III) and Tb(III) hydroxide and oxide nanostructures

Youngku Sohn*

Department of Chemistry, Yeungnam University, Gyeongsan, Gyeongbuk 712-749, South Korea

Received 2 March 2013; accepted 5 May 2013
Available online 14 May 2013

Abstract

Au nanoparticles were embedded in one-dimensional Eu(III) and Tb(III) hydroxide and oxide nanostructures, and the Au doping effect was understood by contour mapping 2D and 3D-photoluminscecne profiles. Photoluminescence intensity was commonly quenched by dipole–dipole coupling between Au NPs and luminescent centers. The $^5D_0 \rightarrow {}^7F_J$ emission of Eu(III) was observed by a direct excitation of Eu(III), while the emission was further quenched upon annealing, and only observed by an indirect excitation. The $^5D_4 \rightarrow {}^7F_J$ emission of Tb(III) was seen before annealing. Upon annealing, the emission was totally quenched, and a broad emission peak was observed at 550 nm.

Keywords: Europium; Terbium; Photoluminescence; Au nanoparticle; Quenching

1. Introduction

Bulk gold (Au) shows very unique/abnormal properties as the size reaches to nanometer region, where it is catalytic, and strongly absorbs visible light (called surface plasmon absorption) [1–3]. Applications using Au nanoparticles (NPs) are explosive and wide from catalysts to bioluminescent sensors [4–8]. Presence of Au NPs near active media (e.g., TiO_2 in solar cell, and luminescent materials) give a positive or a negative effect on efficiency [9–16]. Nahm et al. incorporated 100 nm Au NPs into TiO_2 for dye-sensitized solar cells (DSSCs), and obtained increased power conversion efficiency attributed to surface plasmon absorption of Au [9]. Lin et al. examined the luminescence of $Eu(TTFA)_3$ in PMMA, and found a decrease in luminescence intensity and lifetime with increasing Au NPs [10]. Haldar and Patra observed a decrease and an increase in luminescence intensity for a Eu complex modified with Au and Au–ZnO core–shell NPs, respectively [12]. A drastic enhancement of photoluminescence from Eu(III)-doped GeO_2–Bi_2O_3 glasses was observed upon Au NPs incorporation, reported by Kassab et al. [13]. This enhancement was attributed to an energy transfer from metal NPs to luminescent Eu(III) ions, and a confined electric magnetic field [13,14].

In this paper, to further clearly understand the effect of doped Au NPs on photoluminescence I incorporate Au NPs into Eu(III) and Tb(III) hydroxide and oxide nanorods, and examine change in photoluminescence by 2D and 3D-photoluminescence contour mapping technique. Eu(III) and Tb(III) are good model luminescent ions for red and green emission, respectively [17].

2. Material and methods

Au-doped (1 mol%) Eu(III) and Tb(III) hydroxide nanorods were synthesized by a hydrothermal method as follows. I mixed 1.0 mL of 0.01 M Au chloride (0.1 M) solution and 10 mL of 0.1 M Eu(III) or Tb(III) nitrate solution, added 15.0 mL of Millipore water, stirred for a while, and added an appropriate amount of ammonia solution to obtain precipitates. The solution was then transferred to a Teflon bottle, and placed in a 120 °C oven for 12 h. The final white precipitates were centrifuged and washed repeatedly with water and ethanol, and fully dried at 80 °C in a dry oven. The surface morphology was characterized by scanning electron microscopy (SEM, Hitachi SE-4800).

*Corresponding author. Tel.: +82 53 810 2354; fax: +82 53 810 4613.
E-mail address: youngkusohn@ynu.ac.kr

0272-8842/$ - see front matter © 2013 Elsevier Ltd and Techna Group S.r.l. All rights reserved.
http://dx.doi.org/10.1016/j.ceramint.2013.05.016

Diffuse reflectance absorption spectra were taken using a Cary5000 UV–vis spectrophotometer. The X-ray diffraction (XRD) patterns of the powder samples were taken using a PANalytical X'Pert Pro MPD diffractometer with Cu Kα radiation. Contour maps of 2D and 3D-photoluminescence spectra were taken using a SCINCO FluoroMate FS-2.

3. Results and discussion

Fig. 1 shows the SEM images of as-prepared Au-doped Eu(III) and Tb(III) samples synthesized by a hydrothermal method. As shown, the Au-doped Eu(III) particles show one-dimensional nanorods with sub-micron size long and ~50 nm wide. It was reported that Eu(III) hydroxide commonly shows one dimensional structure grown along [001] direction [18]. For Au-doped Tb(III) sample, the rods are slightly longer, but thinner than the Eu nanorods. Upon annealing to 700 °C, the nanorods show no critical change in morphology (not shown), but the white Eu sample changes to violet color, and the color of the Tb sample turn into brown as shown in Fig. 1.

Fig. 2 shows the XRD patterns of as-prepared Au-doped Eu (III) and Tb(III) samples. For the Eu sample, the XRD patterns are in good accord with those of hexagonal (P63/m) (JCPDS 01-083-2305) $Eu(OH)_3$ ($a=b=6.35$ Å, $c=3.65$ Å, and $\alpha=\beta=90°$, $\gamma=120°$). The (100) plane peak is located at $2\theta=16.1$, and other planes are assigned on the peaks [18,19]. Upon annealing, the XRD peaks are totally changed, and the major four peaks are located at 2θ=28.5°, 33.0°, 47.4°, and 56.2° attributed to (222), (400), (440), and (622) planes, respectively. All the XRD peaks are similar to those of cubic (la-3) (JCPDS 043-1008) Eu_2O_3 [18,19]. For the as-prepared Tb sample, the XRD peaks are very similar to those of the as-prepared Eu sample, and also to hexagonal (P63/m) (JCPDS 01-070-0530) $Tb(OH)_3$. ($a=b$=6.31 Å, c=3.60 Å, and $\alpha=\beta$=90° Å, γ=120°) [20]. Upon annealing the sample, the major three peaks are positioned at $2\theta=38.2°$, 44.6°, and 64.7°, tentatively assigned to (111), (200), and (220) planes of cubic (JCPDS 01-075-0275) $TbO_{1.81}$, respectively. The XRD peaks of Au are weakly observed, and the peak at $2\theta=38.2°$ is assigned to (111) plane of metallic Au with cubic (Fm-3m) structure (JCPDS 01-089-3697).

Fig. 3 shows the UV–vis absorption spectra of reference undoped $Eu(OH)_3$ and $Tb(OH)_3$ nanorods, and Au-doped $Eu(OH)_3$ and $Tb(OH)_3$ nanorods before and after 700 °C annealing. The y-axis was converted from the diffuse reflectance by the Kubelka–Munk method. A sharp peak at 395 nm seen from the spectrum of reference $Eu(OH)_3$ nanorod is attributed to $^5L_6 \leftarrow {}^7F_0$ transition of Eu(III), and the neighboring peaks to $^5G_6 \leftarrow {}^7F_0$ transition. Upon doping Au, the absorption peaks become very broad, and show enhanced absorption in the visible region for the $Eu(OH)_3$ and $Tb(OH)_3$ nanorods. Upon annealing the samples, the absorption in the visible region is further greatly enhanced for the two samples.

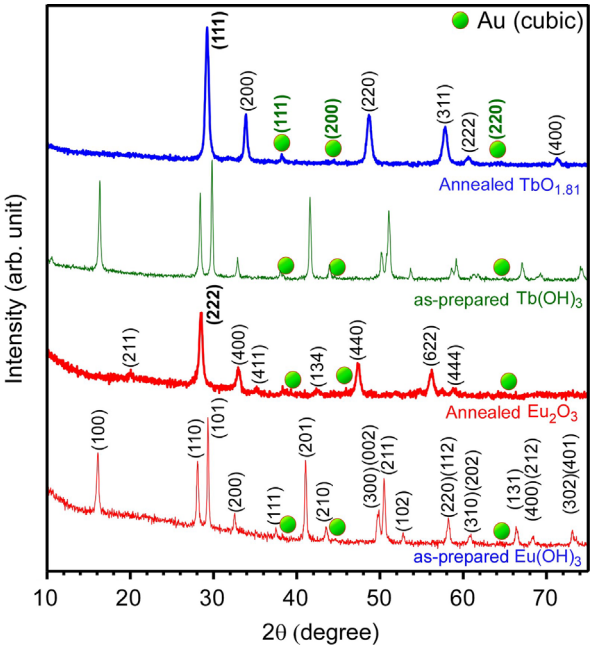

Fig. 2. Powder X-ray diffraction patterns of as-prepared and annealed Au-doped Eu(III) and Tb(III) samples.

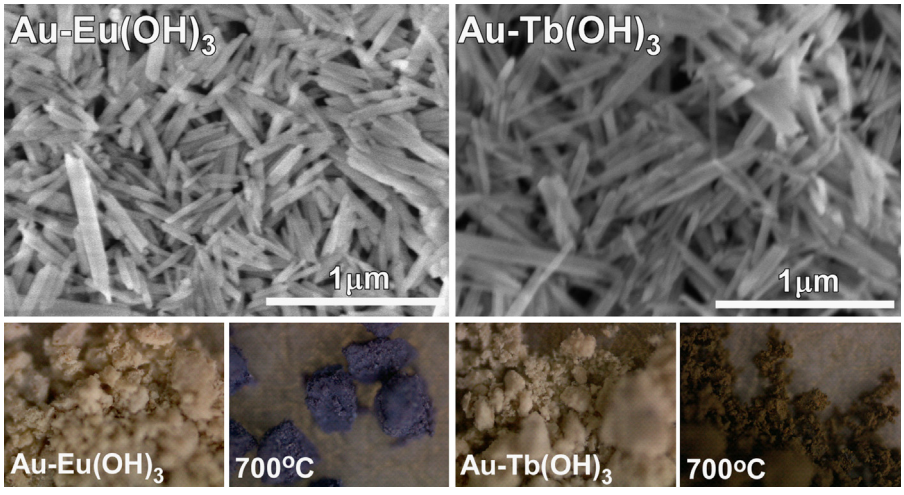

Fig. 1. SEM images of as-prepared and annealed Au-doped Eu(III) and Tb(III) samples. Optical microscope images of as-prepared and 700 °C-annealed samples. (For interpretation of the references to color in this figure, the reader is referred to the web version of this article.)

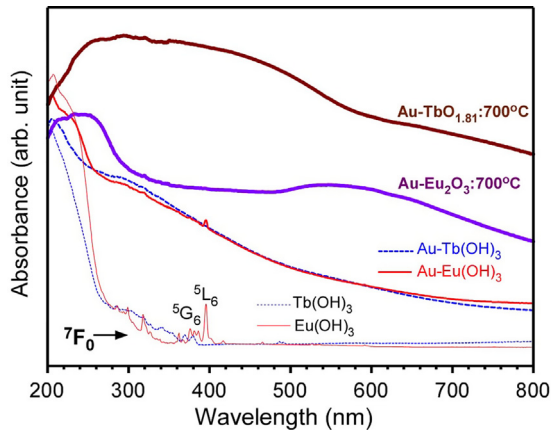

Fig. 3. Diffuse reflectance UV–vis absorption spectra of as-prepared and annealed Au-doped Eu(III) and Tb(III) samples, comparison with those (used only for comparison) of undoped as-prepared samples. The UV–vis absorption spectra of reference samples will be described in detail elsewhere by the author.

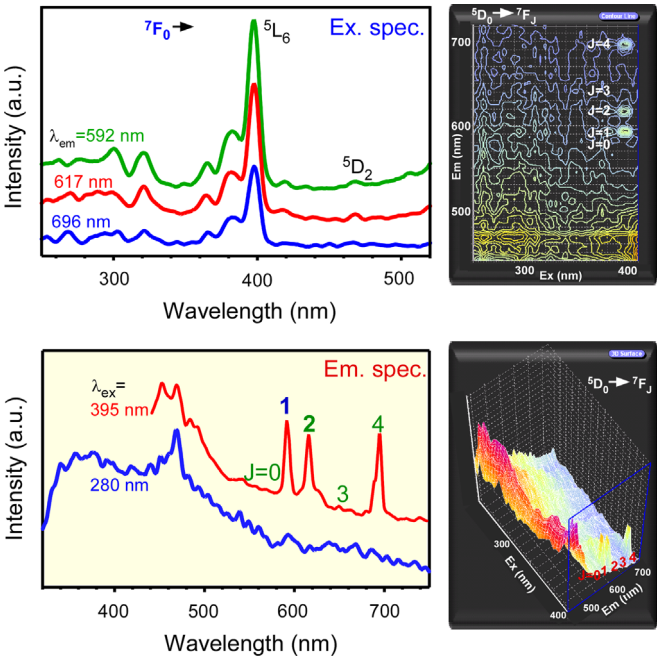

Fig. 4. Excitation and emission spectra as-prepared Au-doped $Eu(OH)_3$ nanorod, and the corresponding 2D and 3D-photoluminescence contour map profiles.

Especially, for the annealed Au-doped Eu(III) sample (or Au–Eu_2O_3), a broad bump is clearly seen at 550 nm. This is commonly attributed to a surface plasmon absorption peak of Au NP [13]. The violet color (in Fig. 1) of the powder sample is attributed to the broad absorption at 550 nm [21]. For the annealed Au-doped Tb sample (or Au–Tb oxide), the strongly enhanced absorption in the 250–800 nm region is mainly due to Tb oxide itself, and partly due to Au NPs. Upon annealing undoped $Tb(OH)_3$ nanorod, it was also observed that the color changes to brown, and the UV–vis absorption (not shown here) is greatly enhanced in the 250–800 nm region.

Fig. 4 shows the photoluminescence (excitation and emission) spectra, 2D and 3D-photoluminescence contour maps of as-prepared Au-doped $Eu(OH)_3$ nanorod. For the excitation spectra taken at various emission wavelengths of 592, 617, and 696 nm, the excitation spectra are all very similar with a sharp major peak at 395 nm. This is a characteristic excitation transition of Eu(III), corresponding to direct $^5L_6 \leftarrow {}^7F_0$ excitation. A weak peak at 465 nm is attributed to direct $^5D_2 \leftarrow {}^7F_0$ transition. For the emission spectra taken at 395 nm excitation, direct $^5L_6 \leftarrow {}^7F_0$ excitation of Eu^{3+} energy level, the peaks in 550–750 nm region are very similar to those (not shown here) found for undoped $Eu(OH)_3$ with a hexagonal site symmetry. But, the intensity is decreased upon Au NP doping. The quenching (or decrease) of luminescence intensity has generally been understood by non-radiative energy transfer, associated with dipole (electron–hole pair in luminescent center)-dipole (metal surface) coupling [4,10]. Here, the doped Au NP quenches the luminescence. The emission peaks are attributed to $^5D_0 \rightarrow {}^7F_J$ (J=0–4) transitions of Eu(III) ion [17]; $^5D_0 \rightarrow {}^7F_0$ (580 nm, extremely weak, electric dipole transition), $^5D_0 \rightarrow {}^7F_1$ (592 nm, strong, magnetic dipole), $^5D_0 \rightarrow {}^7F_2$ (616 and 628 nm, strong, electric dipole), $^5D_0 \rightarrow {}^7F_3$ (651 nm, weak, electric dipole), and $^5D_0 \rightarrow {}^7F_4$ (691 and 697 nm, strong, electric dipole). In the 2D-contour lines, it is seen that the emission of Eu(III) is localized at an excitation of 395 nm. A much broader and stronger peak is found at 460 nm, which was not observed for undoped $Eu(OH)_3$. This is possibly due to surface defect-related levels. The broad peak is increased by doping guest (Au) metals. At an excitation wavelength of 280 nm (not a direct transition from $^7F_0$ ground state), no $^5D_0 \rightarrow {}^7F_J$ (J=0,1,2,3,4) transitions are observed. Instead, a very broad peak is observed extending from 320 to 550 nm region.

For the annealed Au-doped Eu sample (Au–Eu_2O_3), the excitation and emission spectra, and contour mapped 2D and 3D-photoluminescence profiles are displayed in Fig. 5. For the excitation spectra at 612 nm ($^5D_0 \rightarrow {}^7F_2$) emission, very interestingly the direct excitation transition (e.g., direct $^5L_6 \leftarrow {}^7F_0$ excitation at 395 nm) peaks are totally disappeared. Instead, a broad peak is newly appeared at around 275 nm, attributed to charge transfer from O^{2-} (2p) to Eu^{3+} (4f) [22,23]. At an excitation of 280 nm, the broad peak at around 380 nm is relatively enhanced, the emission peak at 612 nm ($^5D_0 \rightarrow {}^7F_2$) is newly observed by the indirect excitation transition of 280 nm. Before annealing, the $^5D_0 \rightarrow {}^7F_2$ emission peak is not observed by the excitation of 280 nm. Other $^5D_0 \rightarrow {}^7F_J$ (J=0,1,3,4) emission transitions are greatly suppressed, mainly due to change in site symmetry of Eu(III) from hexagonal to cubic, as discussed above. It should be emphasized here that by a direct excitation transition of 395 nm, no characteristic emission of Eu(III) is observed. For the photoluminescence (not shown) of undoped Eu_2O_3, the emission peaks by a direct excitation were strongly observed, and the emission of $^5D_0 \rightarrow {}^7F_2$ transition was dominant. Upon annealing, it appears that Au NPs form a good coupling (or wave function mixing by enhanced interfacial contact upon annealing) with luminescent Eu^{3+} center by a direct excitation to quench luminescence process. Therefore, the emission of Eu(III) is more plausibly

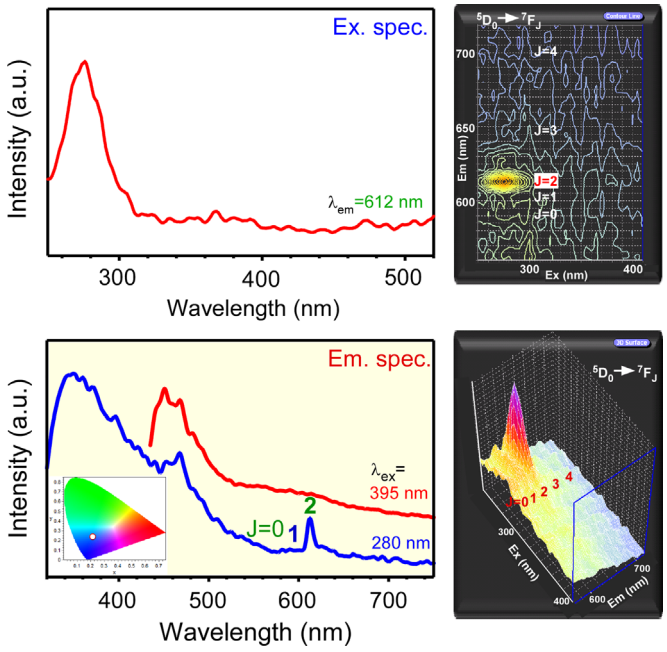

Fig. 5. Excitation and emission spectra of annealed Au-doped Eu_2O_3, and the 2D and 3D-photoluminescence contour map profiles. Inset shows a color coordinate of the emission excited at 280 nm.

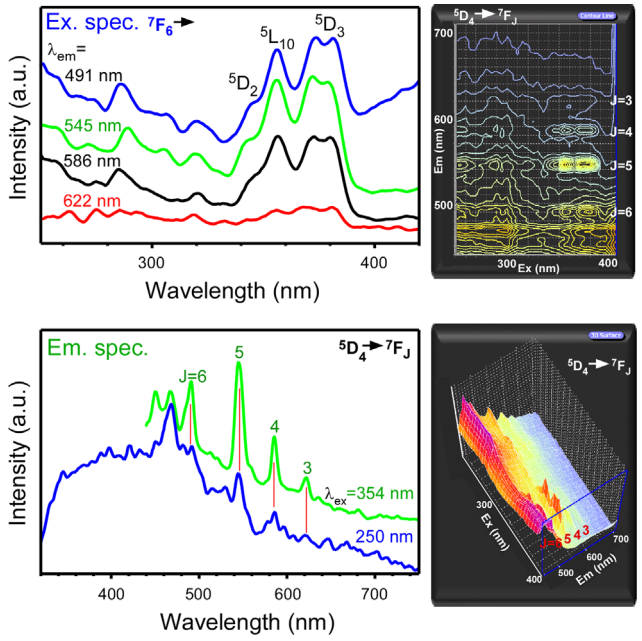

Fig. 6. Excitation and emission spectra of as-prepared Au-doped $Tb(OH)_3$ nanorod, and the corresponding 2D and 3D-photoluminescence contour map profiles.

occurred by an indirect transition than by a direct excitation transition. In addition, the luminescence intensity is decreased by 2.5 × upon annealing due to a decrease in distance between Au NP and luminescent center. Since annealing commonly reduces volume, intuitively the distance will be decreased.

Fig. 6 shows the excitation and emission spectra, 2D and 3D-photoluminescence contour maps of as-prepared Au-doped $Tb(OH)_3$ nanorod. The excitation spectra at various emission wavelengths (491, 545, 586, and 622 nm; $^5D_4 \rightarrow {}^7F_J$, where $J=6,5,4,3$, respectively) are very similar, and show all the characteristic peaks of Tb(III), e.g., $^5D_3 \leftarrow {}^7F_6$, $^5L_{10} \leftarrow {}^7F_6$, and $^5D_2 \leftarrow {}^7F_6$ transitions. This indicates that the characteristic photoluminescence of Tb(III) is very similar for a direct excitation of Tb(III). At two excitation wavelengths, 250 (indirect) and 354 nm (direct), emission spectra were recorded. At a direct excitation of 354 nm, sharp emission peaks are observed in the region from 450 to 650 nm. The emission peaks are attributed to $^5D_4 \rightarrow {}^7F_J$ ($J=6,5,4,3$) transitions of Tb (III) ion [24–26]; $^5D_4 \rightarrow {}^7F_6$ (491 nm), $^5D_4 \rightarrow {}^7F_5$ (545 nm), $^5D_4 \rightarrow {}^7F_4$ (586 nm), and $^5D_4 \rightarrow {}^7F_3$ (622 nm). The 2D and 3D-contour maps further clearly show the emission profiles of Au-doped $Tb(OH)_3$ nanorod. At an indirect excitation of 250 nm, a broad band appears at around 450 nm, plausibly due to defect-related levels. The $^5D_4 \rightarrow {}^7F_J$ emission peaks are greatly reduced.

Upon annealing, the excitation spectrum is drastically changed, as displayed in Fig. 7. The characteristic excitation (e.g., $^5L_{10} \leftarrow {}^7F_6$) peaks of Tb(III) are totally disappeared. The peak at 300 nm is plausibly due to a charge transfer between O (2p) and Tb (4f). In the emission spectra, no characteristic sharp emission ($^5D_4 \rightarrow {}^7F_J$) of Tb(III) is seen, and instead, a broad emission peak is observed at 550 nm. Change in 2D and 3D-contour maps is clearly seen before (Fig. 6) and after (Fig. 7) thermal annealing. These excitation and emission properties are very similar to those (not shown) observed for undoped annealed Tb oxide sample, except a photoluminescence quenching by Au NP.

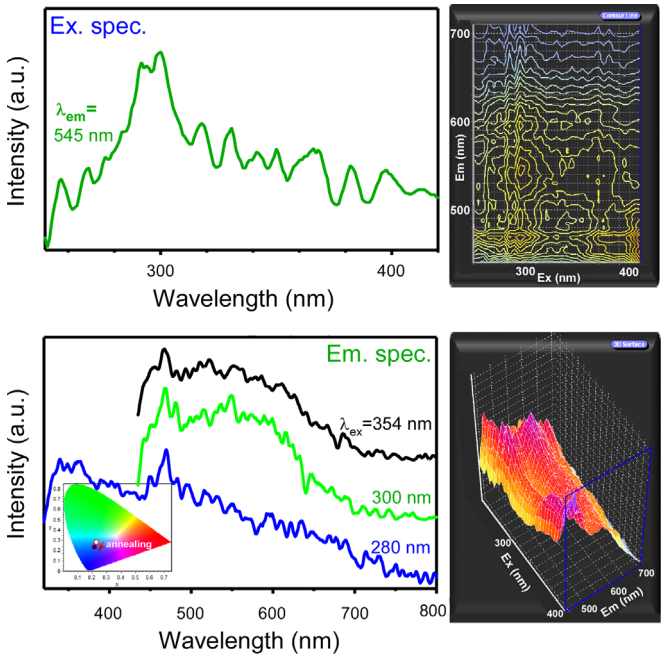

Fig. 7. Excitation and emission spectra of annealed Au-doped Tb oxide sample, and the corresponding 2D and 3D-photoluminescence contour map profiles. Inset shows a color coordinate of the emission spectra excited at 354 nm before and after annealing; the color shifts to a bluer region. (For interpretation of the references to color in this figure legend, the reader is referred to the web version of this article.)

4. Conclusions

Au-doped Eu(III) and Tb(III) hydroxide and oxide nanorods were prepared by a hydrothermal method. By contour mapping 2D and 3D-photoluminescence profiles, it was further clearly understood photoluminescence of Eu(III) and Tb (III) affected by Au NPs. Photoluminescence was commonly quenched by doping Au NP. The intensity was further quenched by thermal annealing. For Au-doped $Eu(OH)_3$ nanorod, the $^5D_0 \rightarrow {}^7F_J$ emission of Eu(III) was observed by a direct excitation of Eu(III). For Au-doped Eu_2O_3 nanorod, the emission was further quenched, and observed only by an indirect excitation. For Au-doped $Tb(OH)_3$ nanorod, the $^5D_4 \rightarrow {}^7F_J$ emission of Tb(III) was observed. Upon annealing, the characteristic sharp emission peaks were totally quenched, and instead a broad emission peak was observed at 550 nm.

Acknowledgment

This work was supported by the National Research Foundation of Korea (NRF) grant funded by the Korea government (MEST) (No. 2012-005645).

References

[1] M. Chen, D.W. Goodman, Catalytically active gold on ordered titania supports, Chemical Society Review 37 (2008) 1860–1870.
[2] S. Eustis, M.A. El-Sayed, Why gold nanoparticles are more precious than pretty gold: noble metal surface plasmon resonance and its enhancement of the radiative and nonradiative properties of nanocrystals of different shapes, Chemical Society Review 35 (2006) 209–217.
[3] B. Hvolbak, T.V.W. Janssens, B.S. Clausen, H. Falsig, C.H. Christensen, J.K. Nørskov, Catalytic activity of Au nanoparticles, Nano Today 2 (2007) 14–18.
[4] J. Lingab, C.Z. Huang, Energy transfer with gold nanoparticles for analytical applications in the fields of biochemical and pharmaceutical sciences, Analytical Methods 2 (2010) 1439–1447.
[5] L. Dykman, N. Khlebtsov, Gold nanoparticles in biomedical applications: recent advances and perspectives, Chemical Society Review 41 (2012) 2256–2282.
[6] E.E. Bedford, J. Spadavecchia, C.-M. Pradier, F.X. Gu, Surface plasmon resonance biosensors incorporating gold nanoparticles, Macromolecular Bioscience 12 (2012) 724–739.
[7] S. Comby, T. Gunnlaugsson, Luminescent lanthanide-functionalized gold nanoparticles: exploiting the interaction with bovine serum albumin for potential sensing applications, ACS Nano 5 (2011) 7184–7197.
[8] H. Nabika, S. Deki, Enhancing and quenching functions of silver nanoparticles on the luminescent properties of europium complex in the solution phase, Journal of Physical Chemistry B 107 (2003) 9161–9164.
[9] C. Nahm, H. Choi, J. Kim, D.-R. Jung, C. Kim, J. Moon, B. Lee, B. Park, The effects of 100 nm-diameter Au nanoparticles on dye-sensitized solar cells, Applied Physics Letters 99 (2001) 253107.
[10] C. Lin, M.T. Berry, P.S. May, Influence of colloidal-gold films on the luminescence of $Eu(TTFA)_3$ in PMMA, Journal of Luminescence 130 (2010) 1907–1915.
[11] J. Zhu, SPR induced quenching of the $5D_1 \rightarrow 7F_1$ emission of Eu^{3+} doped gold colloids, Physics Letters A 341 (2005) 212–215.
[12] K.K. Haldar, A. Patra, Fluorescence enhancement and quenching of Eu^{3+} ions by Au–ZnO core–shell and Au nanoparticles, Applied Physics Letters 95 (2009) 063103.
[13] L.R.P. Kassab, D.S. da Silva, R. de Almeida, C.B. de Araujo, Photoluminescence enhancement by gold nanoparticles in Eu^{3+} doped GeO_2–Bi_2O_3 glasses, Applied Physics Letters 94 (2009) 101912.
[14] L.R.P. Kassab, D.S. da Silva, C.B. de Araujo, Influence of metallic nanoparticles on electric–dipole and magnetic–dipole transitions of Eu^{3+} doped germanate glasses, Journal of Applied Physics 107 (2010) 113506.
[15] M. Eichelbaum, K. Rademann, A. Hoell, D.M. Tatchev, W Weigel, R. Stoßer, G. Pacchioni, Photoluminescence of atomic gold and silver particles in soda–lime silicate glasses, Nanotechnology 19 (2008) 135701.
[16] G. An, C. Yang, Y. Zhou, X. Zhao, Plasmon-enhanced photoluminescence from TiO_2:Sm^{3+}:Au nanostructure, Physica Status Solidi A 209 (2012) 2583–2588.
[17] J.-C.G. Bunzli, Luminescent Probes, in: J.-C.G. Bunzli, G.R. Choppin (Eds.), Lanthanide Probes in Life, Chemical and Earth Sciences, Elsevier, Amsterdam, 1989 (Chapter 7).
[18] Z. Xu, C. Li, P. Yang, Z. Hou, C. Zhang, J. Lin, Uniform $Ln(OH)_3$ and Ln_2O_3 (Ln=Eu, Sm) submicrospindles: facile synthesis and characterization, Crystal Growth and Design 9 (2009) 4127–4135.
[19] N. Du, H. Zhang, B. Chen, J. Wu, D. Li, D Yang, Low temperature chemical reaction synthesis of single-crystalline $Eu(OH)_3$ nanorods and their thermal conversion to Eu_2O_3 nanorods, Nanotechnology 18 (2007) 065605.
[20] Q. Mu, Y. Wang, A simple method to prepare $Ln(OH)_3$ (Ln=La, Sm, Tb, Eu, and Gd) nanorods using CTAB micelle solution and their room temperature photoluminescence properties, Journal of Alloys and Compounds 509 (2011) 2060–2065.
[21] Y. Do, J.-S. Choi, S.K. Kim, Y. Sohn, The interfacial nature of TiO_2 and ZnO nanoparticles modified by gold nanoparticles, Bulletin of the Korean Chemical Society 31 (2010) 2170–2174.
[22] G. Wakefield, H.A. Keron, P.J. Dobson, J.L. Hutchison, Synthesis and properties of Sub-50-nm europium oxide nanoparticles, Journal of Colloid and Interface Science 215 (1999) 179–182.
[23] F. Yanga, Y. Lianga, M. Liub, X. Li, N. Wang, Z. Xi, Enhanced red-emitting by charge compensation in Eu^{3+}-activated Ca_2BO_3Cl phosphors, Ceramics International 38 (2012) 6197–6201.
[24] N. Du, H. Zhang, X. Ma, D.S. Li, D. Yang, Controllable chemical reaction synthesis of $Tb(OH)_3$ nanorods and their photoluminescence property, Materials Letters 63 (2009) 1180–1182.
[25] A.B. Panda, G. Glaspell, M.S. El-Shall, Microwave synthesis and optical properties of uniform nanorods and nanoplates of rare earth oxides, Journal of Physical Chemistry C 111 (2007) 1861–1864.
[26] G. Wakefielda, H.A. Kerona, P.J. Dobsona, J.L. Hutchison, Structural and optical properties of terbium oxide nanoparticles, Journal of Physics and Chemistry of Solids 60 (1999) 503–508.